ACS APPLIED MATERIALS & INTERFACES

Letter

www.acsami.org

Tailoring $Mg_xMn_{1-x}Fe_2O_4$ Superparamagnetic Nanoferrites for Magnetic Fluid Hyperthermia Applications

Minhong Jeun,[†,‡] Sungwook Park,[†] Gun Hyuk Jang,[†,‡] and Kwan Hyi Lee*[,†,‡]

[†]Biomedical Research Institute, Korea Institute of Science and Technology (KIST), Seoul 136-791, Republic of Korea

[‡]Department of Biomedical Engineering, Korea University of Science and Technology (UST), Seoul 136-791, Republic of Korea

Supporting Information

ABSTRACT: A superparamagnetic nanoferrite (SPNF) with high magnetic moment, AC magnetically induced heating (AC-heating) capacity, and good biocompatibility is the most vital part of magnetic fluid hyperthermia for utilizing it in the clinics. Herein, we precisely tune magnetic properties and AC-heating characteristics of $Mg_xMn_{1-x}Fe_2O_4$ SPNF via chemically controlling the cations' concentration and distribution to develop a tailored $Mg_xMn_{1-x}Fe_2O_4$ SPNF as a potential magnetic fluid hyperthermia agent. The magnetic and AC-heating characteristics of the tailored $Mg_xMn_{1-x}Fe_2O_4$ SPNF are strongly dependent on the Mg/Mn cations' concentration and distribution, and $Mg_{0.285}Mn_{0.715}Fe_2O_4$ SPNF exhibits the highest saturation magnetization and AC-heating capacity as well as high biocompatibility.

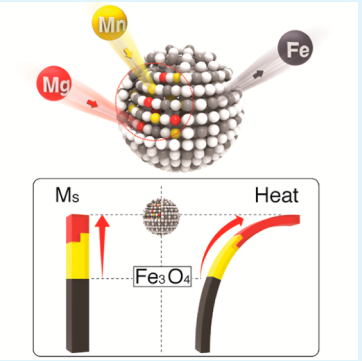

KEYWORDS: *nanoferrite, superparamagnetic particle, $MgMnFe_2O_4$, nanofluid, magnetic hyperthermia*

Magnetic fluid hyperthermia (MFH) using superparamagnetic nanoferrites (SPNFs) has been drawing huge attraction in cancer clinics due to its promising biomedical features to realize both *in vivo* targeting cancer cells and an effective local therapeutic heating of cancer cells under the applied AC magnetic field (Scheme 1).[1−9] To completely eliminate cancer cells with minimized systemic side effects and toxic problems,[10−12] the SPNFs have to satisfy some crucial requirements.[2,13−15] First, the SPNFs need to generate an AC magnetically induced heating temperature (AC-heating, $T_{AC,mag}$) as high as possible at a small concentration (a high specific loss power, SLP). Second, the SPNFs should have a high magnetic susceptibility ($\chi_m = \chi_m' + i\chi_m''$), particularly out-of-phase magnetic susceptibility (χ_m'') directly relevant to the AC-heating characteristics, and a superior biocompatibility. Lastly, it has to generate a high $T_{AC,mag}$ in a physiologically tolerable range of applied magnetic field (H_{appl}), and frequency (f_{appl}). The $H_{appl}f_{appl}$ should be less than 3×10^9 A m^{-1} s^{-1} (generally, H_{appl} < 190 Oe and f_{appl} < 120 kHz).[16] Thus, to address the needs, a great deal of approaches are still put forward to develop new potential SPNFs and enhance the performance of currently considered SPNFs.

Among the numerous SPNFs, the quarterly phase of magnesium−manganese SPNF ($Mg_xMn_{1-x}Fe_2O_4$) is considered to be a potential material for MFH agent applications. The main physical and physiological reasons are that it has negligible Eddy current losses, high Curie temperature, and that both Mg and Mn are biocompatible elements (essential trace nutrients). Mg especially is a cofactor in enzymatic reactions and required for protein and nucleic acid synthesis in cell cycle process, and a part of cytoskeletal and mitochondrial integrity.[17] Furthermore, the magnetic properties (including saturation magnetization, M_s, and magnetic susceptibility) and correspondingly $T_{AC,mag}$ can be readily tuned and significantly improved by precise tailoring of the concentration of Mg cations in tetrahedral (A-site) and octahedral (B-site) sites of $Mg_xMn_{1-x}Fe_2O_4$ SPNF.[18,19]

To synthesize $Mg_xMn_{1-x}Fe_2O_4$ and control the Mg cation concentration, a high temperature (750−1100 °C) is required.[20] However, the same high temperature is also responsible for undesirable large particle size. Therefore, for successful MFH applications, current technologies that utilize $Mg_xMn_{1-x}Fe_2O_4$ SPNFs have to overcome a couple of critical challenges: (1) how to successfully synthesize the superparamagnetic size (phase) of $Mg_xMn_{1-x}Fe_2O_4$ ferrite with an uniform size and size distribution at a lower temperature, (2) how to control the Mg cation concentration of the superparamagnetic $Mg_xMn_{1-x}Fe_2O_4$ ferrite to enhance M_s, $T_{AC,mag}$, as well as SLP.

In this study, we precisely controlled Mg cation concentration at a lower synthesis temperature (<300 °C) to develop a tailored $Mg_xMn_{1-x}Fe_2O_4$ SPNF as a potential MFH agent and determined the optimal chemical composition that shows the highest AC-heating characteristics at a low applied AC magnetic field ($H_{appl}f_{appl} < 1.11 \times 10^9$ $Am^{-1}s^{-1}$) and the significantly improved M_s. The physical correlation between the

Received: August 25, 2014
Accepted: September 19, 2014
Published: September 19, 2014

Scheme 1. Schematic Illustration of in Vivo MFH Using Tailored $Mg_xMn_{1-x}Fe_2O_4$ SPNFs; $Mg_xMn_{1-x}Fe_2O_4$ SPNFs Pass Throughout the Tumor Cell by EPR (Enhanced Permeability and Retention) Effect

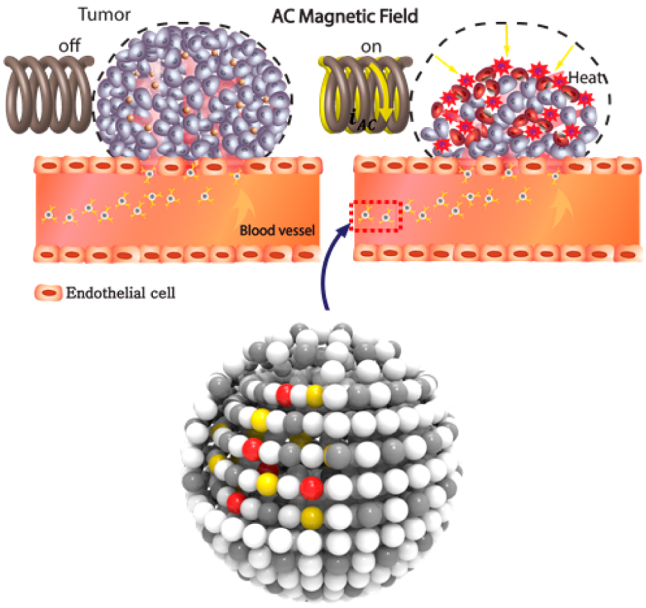

magnetic properties tuned by tailoring the Mg cation's concentration and the $T_{AC,mag}$ characteristics were systematically investigated. In addition, the cell viability of the SPNFs was quantitatively analyzed to evaluate the biocompatibility for in vivo MFH agent applications.

The $Mg_xMn_{1-x}Fe_2O_4$ SPNFs were synthesized at different cation concentrations using a modified thermal decomposition method (Figure 1a).[21] The Mg cation concentration of $Mg_xMn_{1-x}Fe_2O_4$ SPNFs was chemically controlled from x = 0.037 to 0.395 by adjusting the amount of the Mg/Mn precursors and the reducing agent (1,2-hexadecandiol) during the synthesis. The crystal structure, chemical composition, size, and size distribution of the synthesized $Mg_xMn_{1-x}Fe_2O_4$ SPNFs were measured and analyzed. The magnetic properties including M_s, magnetic susceptibility, and minor hysteresis behavior and AC magnetically induced heating characteristics of the solid state and fluid state $Mg_xMn_{1-x}Fe_2O_4$ SPNFs were systematically investigated. In addition, the correlation between the cation concentration and the magnetic and AC-heating characteristics was physically investigated (see detailed descriptions of experimental procedure in the Supporting Information.)

Prior to investigating the magnetic properties and AC-heating characteristics, the crystal structure, size, and size distribution of the $Mg_xMn_{1-x}Fe_2O_4$ nanoferrites were analyzed. Figure 1 (b) shows the XRD patterns of the $Mg_xMn_{1-x}Fe_2O_4$ (x = 0.037−0.395) nanoferrites. The XRD patterns demonstrate that the $Mg_xMn_{1-x}Fe_2O_4$ nanoferrites have a single phase cubic spinel ferrite structure and do not exhibit any undesirable crystalline phase. The absence of any undesirable peaks in the XRD patterns demonstrates that the $Mg_xMn_{1-x}Fe_2O_4$ nanoferrites are phase pure. All the peaks shown in Figure 1a are well-matched with the standard JCPDS data.[22] The average particle size was estimated using Scherrer's formula.[23] The average size of $Mg_xMn_{1-x}Fe_2O_4$ nanoferrites calculated from the XRD patterns is about 8.2 nm, making it close to the 7.5 nm average size determined by statistical analysis of the HR-

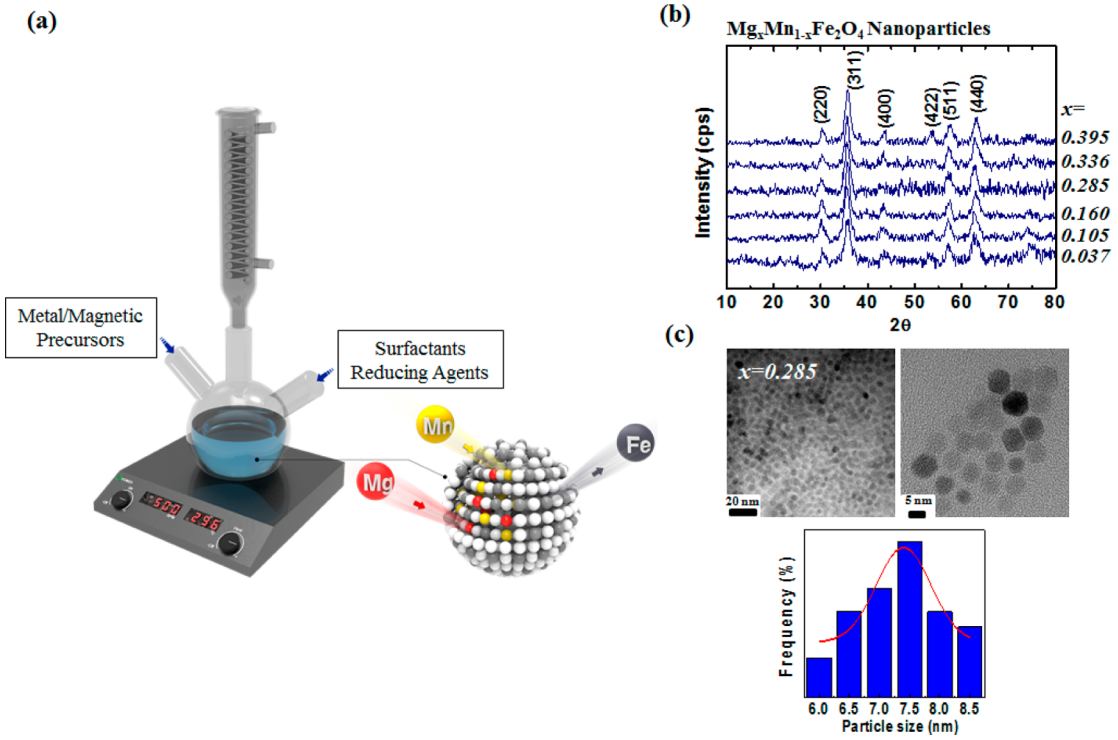

Figure 1. (a) Illustration of the SPNF synthesis: chemically modified thermal decomposition method and tailored $Mg_xMn_{1-x}Fe_2O_4$ SPNF, (b) XRD patterns of $Mg_xMn_{1-x}Fe_2O_4$ nanoferrites for investigating crystal structures, and (c) particle size and its distribution of $Mg_{0.285}Mn_{0.715}Fe_2O_4$ nanoferrites analyzed from HR-TEM images.

dx.doi.org/10.1021/am5057163 | ACS Appl. Mater. Interfaces 2014, 6, 16487−16492

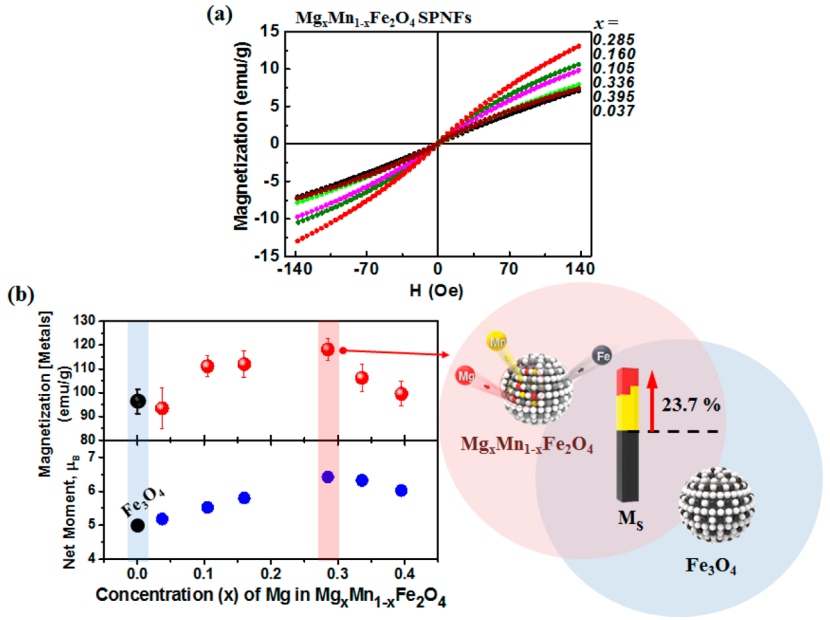

Figure 2. Effect of Mg cation's concentrations on the magnetic properties of $Mg_xMn_{1-x}Fe_2O_4$ SPNFs: (a) minor hysteresis loops and (b) saturation magnetization and net magnetic moment.

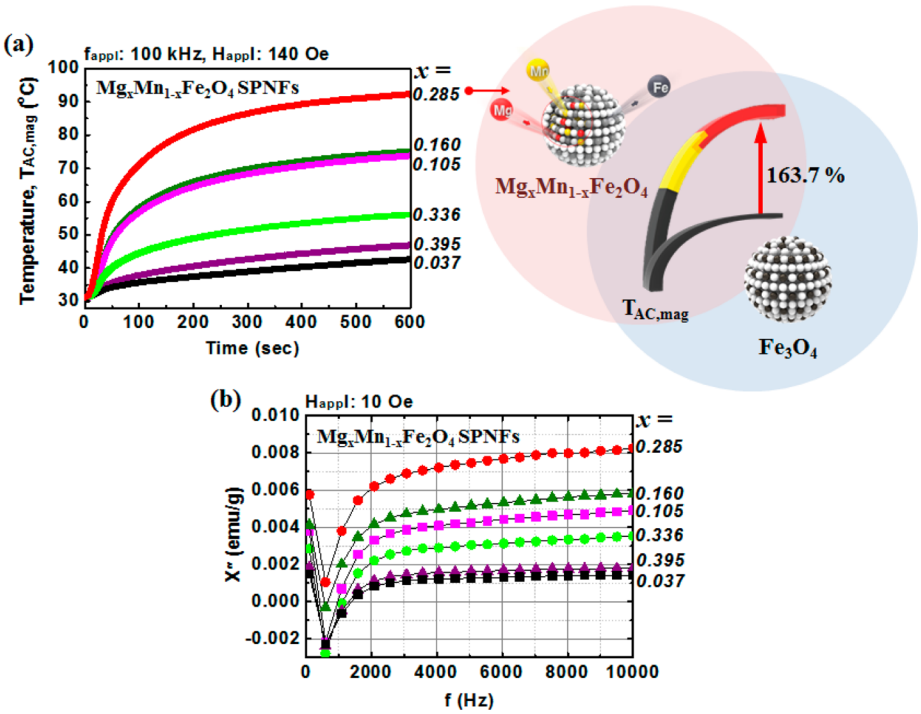

Figure 3. (a) AC magnetically induced heating temperatures and (b) out-of-phase magnetic susceptibilities of $Mg_xMn_{1-x}Fe_2O_4$ SPNFs with different Mg cation concentrations.

TEM images shown in Figure 1c. Figure 1c shows typical HR-TEM images from representative $Mg_{0.285}Mn_{0.715}Fe_2O_4$ nanoferrites. The results clearly show that the particles have a mean particle size of 7.5 nm with a 13.2% standard deviation.

Figure 2a shows the minor hysteresis loops of uncoated (solid state) $Mg_xMn_{1-x}Fe_2O_4$ nanoferrites measured under a H_{appl} of ±140 Oe at room temperature. As clearly can be seen in Figure 2a, all of the prepared $Mg_xMn_{1-x}Fe_2O_4$ nanoferrites do not show any DC magnetic hysteresis loss. The particle size (Figure 1) and the magnetic property analyzed from minor hysteresis loops physically indicate that all the synthesized $Mg_xMn_{1-x}Fe_2O_4$ nanoferrites in this study have superparamagnetic properties.

After confirming the crystal structure and magnetic phase of the synthesized $Mg_xMn_{1-x}Fe_2O_4$ SPNFs, we systematically investigated the dependence of magnetic and AC magnetically induced heating characteristics on the cation concentration of the $Mg_xMn_{1-x}Fe_2O_4$ SPNFs. The results on top of Figure 2b show the M_s of $Mg_xMn_{1-x}Fe_2O_4$ SPNFs at different cation concentrations. As can be seen in the result, the M_s increases

dx.doi.org/10.1021/am5057163 | ACS Appl. Mater. Interfaces 2014, 6, 16487−16492

when the cation concentration also increases. At the cation concentration of Mg = 0.285, the M_s value peaks at 118.22 emu/g and then steadily decreases. The physical and materials-mechanical reason for this pattern is the following. Mg cation's (Mg^{2+}) preference site is the A-site of $Mg_xMn_{1-x}Fe_2O_4$. During synthesis the A-site is the first to be filled. The Mg cation's (Bohr magnetron, $\mu_B = 0$) replaces A-site's Fe cations ($\mu_B = 5$), and the magnetic moment decreases. On the other hand, Mn cation's (Mn^{2+}, $\mu_B = 5$) preference site is the B-site. Therefore, it first replaces B-site's Fe cations ($\mu_B = 5$). Because the μ_B is the same, B-site's magnetic moment stays the same. Consequently, the total net magnetic moment (total net μ_B = $\mu_{B,B\text{-site}} - \mu_{B,A\text{-site}}$) of $Mg_xMn_{1-x}Fe_2O_4$ increases.[24] As the Mg cation concentration increases in A-site the magnetic moment also increases until the Mg cation concentration reaches x = 0.285. From this point on the Mg cations move to B-site and consequently the total net magnetic moment starts to decrease. The lower results in Figure 2b show the calculated μ_B. As can be seen in the results, the calculated μ_B and the experimental μ_B match. These results demonstrate that by modifying the cation concentration, the magnetic property of $Mg_xMn_{1-x}Fe_2O_4$ can be controlled, giving us a SPNF that has a greatly improved magnetic moment than that of the current Fe-nanoferrites. These improved $Mg_xMn_{1-x}Fe_2O_4$ SPNFs are qualified MFH agents that have the ability to increase the magnetic softness, and thus the sensitivity to applied AC magnetic fields.

In the course of studying magnetic property of the $Mg_xMn_{1-x}Fe_2O_4$ SPNFs, the AC-heating characteristics have been studied to see the actual potential of $Mg_xMn_{1-x}Fe_2O_4$ SPNFs applications, and Figure 3a presents $T_{AC,mag}$ of $Mg_xMn_{1-x}Fe_2O_4$ SPNFs at f_{appl} = 100 kHz and H_{appl} = 140 Oe. As it is shown, the value increases in response to incremental change in magnetic moment, and it exhibited the highest value of 92.3 °C with $Mg_{0.285}Mn_{0.715}Fe_2O_4$ SPNFs which possesses the highest magnetic moment. The H_{appl} and f_{appl} used in this study are known to have no harm to human body since they exert low energies ($H_{appl}f_{appl}$ = 1.11 × 10^9 A m^{-1} s^{-1}) suggesting high potentiality of $Mg_{0.285}Mn_{0.715}Fe_2O_4$ SPNFs as a MFH agent.

To explain the physical mechanisms of $Mg_xMn_{1-x}Fe_2O_4$ SPNFs' $T_{AC,mag}$, we investigated the χ''_m (Figure 3 (b)). The main physical mechanism of SPNF's $T_{AC,mag}$ is generally understood that the "Néel relaxation loss power, P_{Neel}", which is directly proportional to the χ''_m, and magnetic softness (eqs 1 and 2).[25−28]

$$\chi_m'' = \chi_0 \frac{2\pi f\tau_{eff}}{1 + (2\pi f\tau_{eff})^2},\ \tau_{eff} \approx \tau_N = \tau_0 \exp\left(\frac{K_a V}{k_B T}\right),$$
$$(\text{soft ferrite: } \tau_N << \tau_B) \rightarrow \chi_m'' \propto \frac{1}{\tau_N} \propto \frac{1}{K_a} \quad (1)$$

$$P_{Neel} = \pi\mu_0\chi_m'' f_{appl} H_{appl}^2 \quad (2)$$

where K_a is magnetic anisotropy, V is volume of SPNFs, $m$is mass of SPNFs, $T_{AC,mag}$ is AC-heating temperature, μ permeability (μ_0, vacuum; μ_r, relative), and τ_{eff}, τ_N, τ_B: effective, Néel, and Brown relaxation time)

As can be seen in Figure 3b, the trend of the χ''_m at different cation concentrations resemble the trends of the magnetic and $T_{AC,mag}$ properties. In addition, at the highest temperature point, the χ''_m value was also the highest, being recorded as $Mg_{0.285}Mn_{0.715}Fe_2O_4$ SPNFs. These χ''_m characteristics, and consequently the M_s, change with the cation concentration and at $Mg_{0.285}Mn_{0.715}Fe_2O_4$ SPNFs produce the largest magnetization, resulting in the greatest magnetic softness (eq 3).[24]

$$M = \chi_m H_{appl}, \quad \chi_m = \chi'_m + i\chi''_m \quad (3)$$

Upon analyzing the cation concentration dependent magnetic and $T_{AC,mag}$ properties of uncoated (solid state) $Mg_xMn_{1-x}Fe_2O_4$ SPNFs, we found that the $Mg_{0.285}Mn_{0.715}Fe_2O_4$ SPNFs showed the most promise as a MFH agent. For investigating the performance of the $Mg_{0.285}Mn_{0.715}Fe_2O_4$ SPNFs in in vivo environments, the SPNFs were coated with lipid[29−32] to form a fluidic state ($Mg_{0.285}Mn_{0.715}Fe_2O_4$@lipid SPNFs).

Figure 4a shows the size, size distribution, and PDI of $Mg_{0.285}Mn_{0.715}Fe_2O_4$@lipid SPNFs. The results obtained from

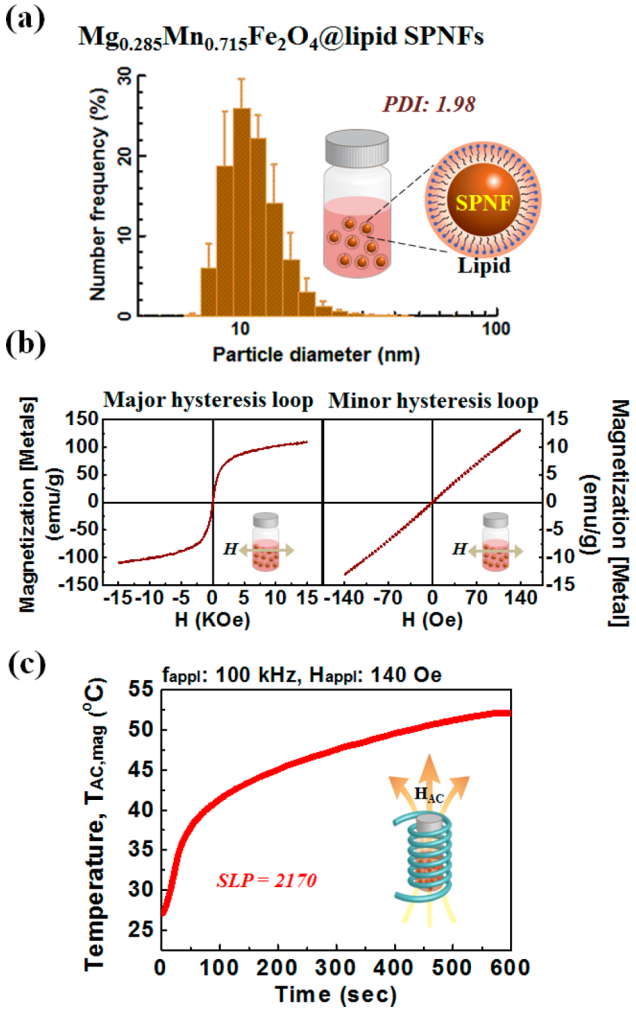

Figure 4. (a) Mean particle size and its distribution of lipid coated $Mg_{0.285}Mn_{0.715}Fe_2O_4$ SPNFs measured by DLS system, (b) major (left) and minor (right) magnetic hysteresis loops of $Mg_{0.285}Mn_{0.715}Fe_2O_4$@lipid SPNFs measured in fluidic status, and (c) AC magnetically induced heating temperature and SLP of $Mg_{0.285}Mn_{0.715}Fe_2O_4$@lipid SPNFs measured in D.I water.

the DLS. $Mg_{0.285}Mn_{0.715}Fe_2O_4$@lipid SPNFs in D.I water have a hydrodynamic diameter averaging 11.8 nm with a standard deviation of 12.4%. The dispersibility of coated nanoparticles can be known from the PDI value, which was 1.98. This value shows that the $Mg_{0.285}Mn_{0.715}Fe_2O_4$@lipid SPNFs are currently

dx.doi.org/10.1021/am5057163 | ACS Appl. Mater. Interfaces 2014, 6, 16487−16492

in a high monodisperse condition. From the DLS results, we are able to know that $Mg_{0.285}Mn_{0.715}Fe_2O_4$@lipid SPNFs have a uniform coating layer, and are spread evenly. This means that in *in vivo* environments, there will be minimal aggregation, leading to smooth transportation to the target cancer cell via blood circulation. The transportation process will have minimal side effects, such as blood clotting, and once the $Mg_{0.285}Mn_{0.715}Fe_2O_4$@lipid SPNFs reach their target, they will be able to efficiently invade the target cancer cell.

After analyzing the both lipid coat status and dispersibilty of $Mg_{0.285}Mn_{0.715}Fe_2O_4$@lipid SPNFs, we investigated their magnetic properties and AC-heating characteristic in D.I water. Figure 4b shows the magnetic properties of $Mg_{0.285}Mn_{0.715}Fe_2O_4$@lipid SPNFs. Analysis of the major hysteresis loop (Figure 4b, left) shows that $Mg_{0.285}Mn_{0.715}Fe_2O_4$@lipid SPNFs have a magnetization value of 109.57 emu/g. This value is similar to the 118.22 emu/g of uncoated (solid state) $Mg_{0.285}Mn_{0.715}Fe_2O_4$ SPNFs. After coating $Mg_{0.285}Mn_{0.715}Fe_2O_4$ with lipid and dispersing them in D.I water, we found the magnetization properties do not change. Analysis of the minor hysteresis loop (Figure 4b, right) reports no DC magnetic hysteresis loss, leading to the conclusion that the $Mg_{0.285}Mn_{0.715}Fe_2O_4$@lipid SPNFs are still maintaining their superparamagnetic phase. From the results above, we were able to see that there were little change in magnetic properties, leading us to the conclusion that there was no clustering inside the D.I water, and that the SPNFs were dispersed properly.

Figure 4c shows the $T_{AC,mag}$ characteristics of the $Mg_{0.285}Mn_{0.715}Fe_2O_4$@lipid SPNFs in D.I water. The concentration of the $Mg_{0.285}Mn_{0.715}Fe_2O_4$@lipid SPNFs was 16 mg/mL, and f_{appl} = 100 kHz, H_{appl} = 140 Oe. Not only $Mg_{0.285}Mn_{0.715}Fe_2O_4$@lipid SPNFs show a high $T_{AC,mag}$ of 52.1 °C at a low concentration and AC magnetic field, but they also give a high SLP value of 2170 W/g. SLP is affected by both nanoparticle concentration and heat-up time. A low SLP is predicts either multiple side effects from use a high concentration of nanoparticle, or cancer cells developing a thermal tolerance due to a slow heat-up time. The high SLP shows that the $Mg_{0.285}Mn_{0.715}Fe_2O_4$@lipid SPNFs can efficiently eliminate cancer cells at low AC magnetic field with use of low concentration. In this way, we demonstrated the potential of $Mg_{0.285}Mn_{0.715}Fe_2O_4$@lipid SPNFs as an in vivo MHF agent that not only has a high $T_{AC,mag}$ and SLP respectively, but also manages to retains its magnetization value and superparamagnetic phase in D.I water.

Finally we tested the cytotoxicity of $Mg_{0.285}Mn_{0.715}Fe_2O_4$ SPNFs before and after they were subject to coating. This was done to see how the SPNFs affect regular cells after they have killed off the cancer cells by measuring metabolic activity of HPDE normal cells. In terms of viability test, HPDE cells exhibit higher sensitivity under toxic environment comparing to that of pancreatic cancer cells. Due to this reason, alamar blue, an alternative reagent to MTT with improved redox reaction outcome, is utilized to measure metabolic activity which reflects viability of the subjected cells. As can be seen in Figure 5, uncoated and lipid coated $Mg_{0.285}Mn_{0.715}Fe_2O_4$ SPNFs showed over 80% cell viability in the 1−100 μg/mL concentration range, leading to the conclusion they are either nontoxic or mod-toxic.

In conclusion, by utilizing a chemically modified thermal decomposition method, $Mg_xMn_{1-x}Fe_2O_4$ SPNFs with precisely manipulated cations synthesized. $Mg_xMn_{1-x}Fe_2O_4$ SPNFs made

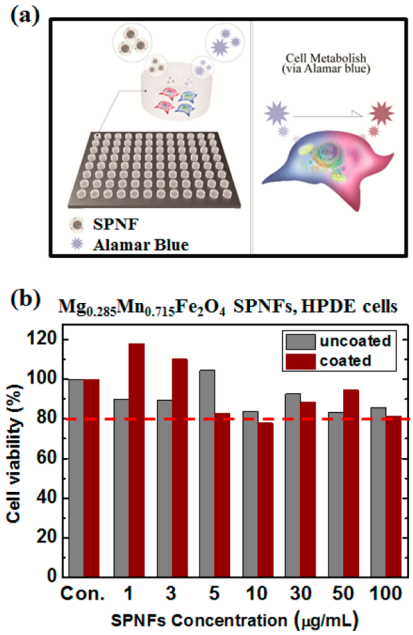

Figure 5. (a) A schematic illustration of Alamar Blue assay for evaluating biocompatibility of $Mn_{0.285}Mn_{0.715}Fe_2O_4$ SPNFs and (b) cell survival rate of uncoated and lipid coated $Mg_{0.285}Mn_{0.715}Fe_2O_4$ SPNFs determined from HPDE cells.

of this systematic synthesis mechanism have magnetic and AC-heating characteristics that are greatly sensitive to the Mg cation concentration. As the Mg cation concentration increases, so does the magnetization and $T_{AC,mag}$ value. This is because the Mg cation replaces the Fe cation at A-site, and thus creates an increase in both total magnetic moment and magnetic softness. As the Mg cation concentration increases above the critical concentration, the Mg cation replaces B-site's Fe cations, causing the total magnetic moment and $T_{AC,mag}$ to decrease. After many attempts, the highest magnetization and $T_{AC,mag}$ values were found to be with $Mg_{0.285}Mn_{0.715}Fe_2O_4$ SPNFs. $Mg_{0.285}Mn_{0.715}Fe_2O_4$@lipid SPNFs especially declared itself a highly possible in vivo MFH agent. Not only did it maintain a superparamagnetic phase in D.I water, but it also had a high magnetization value, a high $T_{AC,mag}$, a high SLP, and a high cell viability as some of its notable characteristics.

■ ASSOCIATED CONTENT

Ⓢ Supporting Information

Synthesis method for superparamagnetic nanoferrite, sample characterization tools, SLP calculation, and in vitro cytotoxicity evaluation are described in detail. This material is available free of charge via the Internet at http://pubs.acs.org.

■ AUTHOR INFORMATION

Corresponding Author

*Tel.: +82 2 958 6804. E-mail: kwanhyi@kist.re.kr.

Notes

The authors declare no competing financial interest.

■ ACKNOWLEDGMENTS

This research was supported by Korea Institute of Science and Technology (Institutional #2E24680, K-GRL #2Z04150) and Basic Science Research Program through the National Research Foundation of Korea (NRF) funded by the Ministry of

Education (2013R1A6A3A04063923). The authors especially thank Mr. Su Chang Mun for his graphical artworks.

REFERENCES

(1) Hayashi, K.; Ono, K.; Suzuki, H.; Sawada, M.; Moriya, M.; Sakamoto, W.; Yogo, T. High-Frequency, Magnetic-Field-Responsive Drug Release from Magnetic Nanoparticle/Organic Hybrid Based on Hyperthermic Effect. *ACS Appl. Mater. Interfaces* **2010**, *2*, 1903−11.

(2) Jordan, A.; Scholz, R.; Wust, P.; Fahling, H.; Felix, R. Magnetic Fluid Hyperthermia (MFH): Cancer Treatment with AC Magnetic Field Induced Excitation of Biocompatible Superparamagnetic Nanoparticles. *J. Magn. Magn. Mater.* **1999**, *201*, 413−419.

(3) Pankhurst, Q. A.; Connolly, J.; Jones, S. K.; Dobson, J. Applications of Magnetic Nanoparticles in Biomedicine. *J. Phys. D Appl. Phys.* **2003**, *36*, R167−R181.

(4) Johannsen, M.; Gneveckow, U.; Eckelt, L.; Feussner, A.; Waldofner, N.; Scholz, R.; Deger, S.; Wust, P.; Loening, S. A.; Jordan, A. Clinical Hyperthermia of Prostate Cancer Using Magnetic Nanoparticles: Presentation of a New Interstitial Technique. *Int. J. Hyperther.* **2005**, *21*, 637−647.

(5) Cervadoro, A.; Cho, M.; Key, J.; Cooper, C.; Stigliano, C.; Aryal, S.; Brazdeikis, A.; Leary, J. F.; Decuzzi, P. Synthesis of Multifunctional Magnetic Nanoflakes for Magnetic Resonance Imaging, Hyperthermia, and Targeting. *ACS Appl. Mater. Interfaces* **2014**, *6*, 12939−46.

(6) Moroz, P.; Jones, S. K.; Gray, B. N. Magnetically Mediated Hyperthermia: Current Status and Future Directions. *Int. J. Nanomed.* **2002**, *18*, 267−284.

(7) Lee, J. H.; Jang, J. T.; Choi, J. S.; Moon, S. H.; Noh, S. H.; Kim, J. W.; Kim, J. G.; Kim, I. S.; Park, K. I.; Cheon, J. Exchange-Coupled Magnetic Nanoparticles for Efficient Heat Induction. *Nat. Nanotechnol.* **2011**, *6*, 418−22.

(8) Laurent, S.; Dutz, S.; Hafeli, U. O.; Mahmoudi, M. Magnetic Fluid Hyperthermia: Focus on Superparamagnetic Iron Oxide Nanoparticles. *Adv. Colloid Interface Sci.* **2011**, *166*, 8−23.

(9) Kobayashi, T. Cancer Hyperthermia Using Magnetic Nanoparticles. *Biotechnol. J.* **2011**, *6*, 1342−1347.

(10) Lacava, L. M.; Garcia, V. A. P.; Kuckelhaus, S.; Azevedo, R. B.; Sadeghiani, N.; Buske, N.; Morais, P. C.; Lacava, Z. G. M. Long-Term Retention of Dextran-Coated Magnetite Nanoparticles in the Liver and Spleen. *J. Magn. Magn. Mater.* **2004**, *272*, 2434−2435.

(11) Hergt, R.; Dutz, S.; Muller, R.; Zeisberger, M. Magnetic Particle Hyperthermia: Nanoparticle Magnetism and Materials Development for Cancer Therapy. *J. Phys.: Condens. Matter* **2006**, *18*, S2919−S2934.

(12) Pradhan, P.; Giri, J.; Banerjee, R.; Bellare, J.; Bahadur, D. Cellular Interactions of Lauric Acid and Dextran-Coated Magnetite Nanoparticles. *J. Magn. Magn. Mater.* **2007**, *311*, 282−287.

(13) Okawa, K.; Sekine, M.; Maeda, M.; Tada, M.; Abe, M.; Matsushita, N.; Nishio, K.; Handa, H. Heating Ability of Magnetite Nanobeads with Various Sizes for Magnetic Hyperthermia at 120 Khz, a Noninvasive Frequency. *J. Appl. Phys.* **2006**, *99*, 08H102−1−08H102−3.

(14) Wust, P.; Gneveckow, U.; Johannsen, M.; Bohmer, D.; Henkel, T.; Kahmann, F.; Sehouli, J.; Felix, R.; Ricke, J.; Jordan, A. Magnetic Nanoparticles for Interstitial Thermotherapy-Feasibility, Tolerance and Achieved Temperatures. *Int. J. Hyperther.* **2006**, *22*, 673−685.

(15) Yoon, T. J.; Lee, H.; Shao, H. L.; Weissleder, R. Highly Magnetic Core-Shell Nanoparticles with a Unique Magnetization Mechanism. *Angew. Chem., Int. Ed.* **2011**, *50*, 4663−4666.

(16) Hergt, R.; Hiergeist, R.; Hilger, I.; Kaiser, W. A.; Lapatnikov, Y.; Margel, S.; Richter, U. Maghemite Nanoparticles with Very High AC-Losses for Application in RF-Magnetic Hyperthermia. *J. Magn. Magn. Mater.* **2004**, *270*, 345−357.

(17) Saris, N. E.; Mervaala, E.; Karppanen, H.; Khawaja, J. A.; Lewenstam, A. Magnesium An Update on Physiological, Clinical and Analytical Aspects. *Clin. Chim. Acta* **2000**, *294*, 21−26.

(18) McCurrie, R. A. *Ferromagnetic Materials: Structure and Properties*; Academic: London, 1994.

(19) Sepelak, V.; Bergmann, I.; Menzel, D.; Feldhoff, A.; Heitjans, P.; Litterst, F. J.; Becker, K. D. Magnetization Enhancement in Nanosized $MgFe_2O_4$ Prepared by Mechanosynthesis. *J. Magn. Magn. Mater.* **2007**, *316*, E764−E767.

(20) Li, F.; Liu, J. J.; Evans, D. G.; Duan, X. Stoichiometric Synthesis of Pure MFe_2O_4 (M = Mg, Co, and Ni) Spinel Ferrites from Tailored Layered Double Hydroxide (Hydrotalcite-Like) Precursors. *Chem. Mater.* **2004**, *16*, 1597−1602.

(21) Sun, S. H.; Zeng, H.; Robinson, D. B.; Raoux, S.; Rice, P. M.; Wang, S. X.; Li, G. X. Monodisperse MFe_2O_4 (M = Fe, Co, Mn) Nanoparticles. *J. Am. Chem. Soc.* **2004**, *126*, 273−279.

(22) Ahmed, M. A. The Effect of Urea-to-Nitrates Ratio on the Morphology and Magnetic Properties of $Mn_{0.8}Mg_{0.2}Fe_2O_4$. *J. Magn. Magn. Mater.* **2010**, *322*, 763−766.

(23) Cullity, B. D. *Elements of X-Ray Diffraction*; Addison-Wesley: Boston, 1956.

(24) Cullity, B. D. and Graham, C. D. *Introduction to Magnetic Materials*, 2nd ed; A John Wiley & Sons, INC., Publication: NJ, 2009.

(25) Lu, Y.; Yin, Y. D.; Mayers, B. T.; Xia, Y. N. Modifying the Surface Properties of Superparamagnetic Iron Oxide Nanoparticles through a Sol-Gel Approach. *Nano Lett.* **2002**, *2*, 183−186.

(26) Hergt, R.; Andra, W.; d'Ambly, C. G.; Hilger, I.; Kaiser, W. A.; Richter, U.; Schmidt, H. G. Physical Limits of Hyperthermia Using Magnetite Fine Particles. *IEEE Trans. Magn.* **1998**, *34*, 3745−3754.

(27) Gupta, A. K.; Gupta, M. Synthesis and Surface Engineering of Iron Oxide Nanoparticles for Biomedical Applications. *Biomaterials* **2005**, *26*, 3995−4021.

(28) Yu, H.; Chen, M.; Rice, P. M.; Wang, S. X.; White, R. L.; Sun, S. H. Dumbbell-Like Bifunctional Au-Fe_3O_4 Nanoparticles. *Nano Lett.* **2005**, *5*, 379−382.

(29) Lee, K. H.; Galloway, J. F.; Park, J.; Dvoracek, C. M.; Dallas, M.; Konstantopoulos, K.; Maitra, A.; Searson, P. C. Quantitative Molecular Profiling of Biomarkers for Pancreatic Cancer with Functionalized Quantum Dots. *Nanomedicine* **2012**, *8*, 1043−1051.

(30) Galloway, J. F.; Winter, A.; Lee, K. H.; Park, J. H.; Dvoracek, C. M.; Devreotes, P.; Searson, P. C. Quantitative Characterization of the Lipid Encapsulation of Quantum Dots for Biomedical Applications. *Nanomedicine* **2012**, *8*, 1190−1199.

(31) Choi, J.; Park, S.; Stojanovic, Z.; Han, H. S.; Lee, J.; Seok, H. K.; Uskokovic, D.; Lee, K. H. Facile Solvothermal Preparation of Monodisperse Gold Nanoparticles and Their Engineered Assembly of Ferritin-Gold Nanoclusters. *Langmuir* **2013**, *29*, 15698−15703.

(32) Hwang, M. P.; Lee, J. W.; Lee, K. E.; Lee, K. H. Think Modular: A Simple Apoferritin-Based Platform for the Multifaceted Detection of Pancreatic Cancer. *ACS Nano* **2013**, *7*, 8167−8174.